Journal for ImmunoTherapy of Cancer

Intratumoral PPT1-positive macrophages determine immunosuppressive contexture and immunotherapy response in hepatocellular carcinoma

Jialei Weng,[1,2] Shaoqing Liu,[1,2] Qiang Zhou,[1,2] Wenxin Xu,[1] Minghao Xu,[1] Dongmei Gao,[1] Yinghao Shen,[1] Yong Yi,[1] Yi Shi,[3] Qiongzhu Dong,[2,4] Chenhao Zhou ,[1,2] Ning Ren [1,2,4]

To cite: Weng J, Liu S, Zhou Q, *et al*. Intratumoral PPT1-positive macrophages determine immunosuppressive contexture and immunotherapy response in hepatocellular carcinoma. *Journal for ImmunoTherapy of Cancer* 2023;**11**:e006655. doi:10.1136/jitc-2022-006655

► Additional supplemental material is published online only. To view, please visit the journal online (http://dx.doi.org/10.1136/jitc-2022-006655).

JW, SL and QZ are joint first authors.

Accepted 11 June 2023

For numbered affiliations see end of article.

Correspondence to
Professor Ning Ren;
ren.ning@zs-hospital.sh.cn

Dr Chenhao Zhou;
zhouchenhao@fudan.edu.cn

ABSTRACT

Background Hepatocellular carcinoma (HCC) is a malignancy with limited treatment options and poor prognosis. Macrophages are enriched in the HCC microenvironment and have a significant impact on disease progression and therapy efficacy. We aim to identify critical macrophages subsets involved in HCC development.

Methods Macrophage-specific marker genes were identified through single-cell RNA sequencing analyses. The clinical significance of macrophages with palmitoyl-protein thioesterase 1 (PPT1) positive was investigated in 169 patients with HCC from Zhongshan Hospital using immunohistochemistry and immunofluorescence. The immune microenvironment of HCC and the functional phenotype of $PPT1^+$ macrophages were explored using cytometry by time-of-flight (CyTOF) and RNA sequencing.

Results Single-cell RNA sequencing analyses revealed that PPT1 was predominantly expressed in macrophages in HCC. Intratumoral $PPT1^+$ macrophages abundance was associated with inferior survival durations of patients and an independent risk factor of prognosis for HCC. High throughput analyses of immune infiltrates showed that $PPT1^+$ macrophage-enriched HCCs were characterized by high infiltration of $CD8^+$ T cells with increased programmed death-1 (PD-1) expression. $PPT1^+$ macrophages exhibited higher galectin-9, CD172a, and CCR2 levels but lower CD80 and CCR7 levels than $PPT1^-$ macrophages. Pharmacological inhibition of PPT1 by DC661 suppressed mitogen-activated protein kinase (MAPK) pathway activity but activated nuclear factor kappa B (NF-κB) pathway in macrophages. In addition, DC661 enhanced the therapeutic efficacy of anti-PD-1 antibody in the HCC mouse model.

Conclusions PPT1 is mainly expressed in macrophages in HCC and promotes immunosuppressive transformation of macrophages and tumor microenvironment. $PPT1^+$ macrophage infiltration is associated with poor prognosis of patients with HCC. Targeting PPT1 may potentiate the efficacy of immunotherapy for HCC.

WHAT IS ALREADY KNOWN ON THIS TOPIC

⇒ Hepatocellular carcinoma (HCC) has a low response to current immunotherapy and there is an urgent need for effective combination strategies and biomarkers. Macrophages have a profound impact on the immune features, therapeutic response, and disease prognosis of HCC due to their highly heterogeneous and plastic phenotypes. However, key macrophage subsets and well-validated markers that can be prognostic classifiers or revealer of microenvironmental characteristics remain largely unknown.

WHAT THIS STUDY ADDS

⇒ In this study, we found that palmitoyl-protein thioesterase 1 (PPT1) is predominantly expressed on macrophages in tumors and associated with the prognosis of patients with HCC. $PPT1^+$ macrophage-enriched HCC is an immunologically 'hot' but immunosuppressive tumor. $PPT1^+$ macrophages exhibit a more immunosuppressive phenotype than $PPT1^-$ macrophages. Our in vivo study showed that PPT1 inhibition by DC661 sensitizes HCC to anti-PD-1 (programmed death-1) therapy.

HOW THIS STUDY MIGHT AFFECT RESEARCH, PRACTICE OR POLICY

⇒ Our study unravels a previously unrecognized role of PPT1 as a therapeutic target and biomarker in HCC, which could be exploited to enhance antitumor immunity and improve immunotherapy management of patients with HCC.

BACKGROUND

Liver cancer remains a global health issue, with the sixth highest incidence and the third highest mortality currently.[1] Hepatocellular carcinoma (HCC) is the most common histological type of primary liver cancer, accounting for 80–90% cases.[2] Despite the fact that a few patients are eligible for curative surgery, most patients with postoperative recurrence and metastases require further treatment.[2] Multikinase inhibitors as first-line recommendation for advanced HCC, only provide a minor extension of overall survival (OS) duration

to patients.[3 4] The advent of immunotherapies such as immune checkpoint blockade (ICB) has already changed the treatment paradigm of liver cancer, but the objective response rate is still less than 20%.[5] In addition, the prognosis evaluation systems such as Barcelona Clinic Liver Cancer staging and tumor-node-metastasis staging do not seem to meet the growing need for patient stratification proposed by novel therapy strategies. Therefore, identification of effective biomarkers that can predict prognosis risk and therapy efficacy for HCC is warranted.

A deeper understanding of the complicated cellular and molecular networks that characterize the tumor immune microenvironment of HCC facilitates the development of new antitumor immune-based therapeutic strategies and predictive biomarkers.[6 7] The function balance between immune effector and immunosuppressive cells, as well as the immune evasion capacity of tumor cells, determines the response rate of ICB.[8] In HCC, macrophages, including resident Kupffer cells and those migrating from the blood circulation, are abundantly enriched in the tumor microenvironment. They can exert antitumor effects such as phagocytosis and antigens presentation, but are also susceptible to re-education into tumor-associated macrophages (TAMs). The highly heterogeneous and plastic phenotype of macrophages can have a dramatic effect on surrounding cells, which in turn affects the balance between antitumor immunity and immune evasion in HCC.[9 10] Hence, a better understanding of the molecular landscapes that characterize TAMs in the HCC microenvironment, and accurate identification of critical macrophages subsets is required for reversing HCC immunosuppressive microenvironment, improving the immunotherapy efficacy, and predicting prognosis. However, well-validated markers of TAMs that can be robust prognostic classifiers or revealer of microenvironmental characteristics remain an unmet need for HCC.

Palmitoyl-protein thioesterase 1 (PPT1), an enzyme catalyzing depalmitoylation processes, has been reported to be upregulated in various cancers and associated with adverse outcomes, including HCC, oral squamous cell carcinoma, and esophageal cancer.[11–13] Notably, PPT1 has been identified as the molecular target of antimalarial compounds such as DQ661 and DC661, and these PPT1 inhibitors can impair cellular lysosomal catabolism through palmitoylated proteins accumulation to inhibit tumor growth and sensitize tumor cells to targeted therapy and immunotherapy.[11 13–16] However, previous studies have focused on the biological effects of PPT1 in tumor cells, while its expression pattern and primary role in the complex microenvironment of HCC remain to be further explored.

Here, by performing high-throughput single-cell analyses, we aim to identify key macrophage subtypes in HCC and reveal their impact on the immune microenvironment landscape and clinical outcome of HCC. We found that PPT1 was predominantly expressed on macrophages in the HCC microenvironment by single-cell RNA sequencing analyses. Besides, patients with HCC with low PPT1 level and low macrophages infiltration experienced the best survival duration. Using cytometry by time-of-flight (CyTOF), we also showed that $PPT1^+$ macrophage-enriched HCC was immunologically 'hot' tumor characterized by high infiltration of T cells with increased programmed death-1 (PD-1) expression, which may have a higher response to ICB. Besides, $PPT1^+$ macrophages exhibited a more immunosuppressive phenotype than $PPT1^-$ macrophages. In vivo pharmacological inhibition of PPT1 by DC661 sensitized HCC to anti-PD-1 therapy. This study provides a new illustration of the immunological relevance and clinical significance of $PPT1^+$ macrophages in HCC.

METHODS

Patients and specimens

Archived tumor and peritumor specimens of 169 patients with HCC who underwent surgical resection at Zhongshan Hospital, Fudan University (Shanghai, China), between January 2009 and January 2010 were collected for this study. In addition, we collected eight fresh HCC tissue specimens for CyTOF examinations. All patients signed the written informed consent and followed our previous inclusion criteria and follow-up schedule.[17] The clinicopathological data was obtained from the electronic medical record system.

In addition, the RNA-sequencing and clinical data of the cancer genome atlas liver hepatocellular carcinoma (TCGA-LIHC) cohort was downloaded from the Genomic Data Commons Data Portal. Transcriptome data was normalized using the 'limma' package in R software before further analyses. The tumor immune infiltration and activity enrichment scores for each sample were assessed by performing single-sample gene set enrichment analysis (ssGSEA) in R software using the 'gsva' package. Besides, the absolute infiltration proportions of various immune cell types were calculated using cell-type identification by estimating relative subsets of RNA transcripts (CIBERSORT) algorithm.

Single-cell RNA sequencing analyses

Single-cell RNA sequencing data of a patient with liver cancer cohort (GSE125449) was obtained from the Gene Expression Omnibus (GEO) website.[18] A total of 3299 cells (Set 1) and 4831 cells (Set 2) of GSE125449 was analyzed. Quality control steps included removal of doublets and cells with >5% mitochondrial gene. Subsequently, after the transcriptome data were normalized and log-transformed, we detected 2000 highly variable genes for further principal component analysis based on the average expression and dispersion of the genes. The first 20 principal components ($p<0.05$) were applied for t-distributed stochastic neighbor embedding (t-SNE) analyses to reveal different single cell subclusters and cell types were annotated automatically using 'singleR' package in R software. The single-cell gene expression was correlated

with reference bulk RNA-sequencing data sets including Human Primary Cell Atlas, Blueprint/ENCODE, Database Immune Cell Expression, Novershtern Hematopoietic, and Monaco Immune. The above analyses were performed using the 'Seurat' package in R software. For macrophage subset analysis, myeloid cells were extracted from Set 1 and Set 2 for clustering and visualized using the Uniform Manifold Approximation and Projection plots. Cells were annotated by myeloid markers (CD68, CD163, C1QC, CLEC9A, S100A8, CD1C, and LAMP3) and macrophage subsets were further analyzed using TAMs markers and M1/M2 signatures.[19]

Immunohistochemistry

Immunohistochemical (IHC) staining was performed on the tissue microarrays containing specimens from the above-mentioned 169 patients with HCC as described in our previous study.[17] Briefly, after deparaffinization and antigen retrieval, the microarrays were incubated sequentially with the indicated primary antibodies (PPT1, Cat. ab89022, Abcam; CD68, Cat.ab213363, Abcam) and horseradish peroxidase (HRP)-conjugated secondary antibody. Later, two pathologists independently evaluated the staining results using a semiquantitative method while maintaining confidentiality of clinical data. The final score was the multiplication of staining intensity (− scored 0, + scored 0~1, ++ scored 1–1.5, +++ scored 1.5–3) and staining area (0–100%) and was ranked into four grades: negative (0%) and weak (0–100%) staining was considered as low expression, while moderate (100–150%) and strong (150–300%) staining was deemed as high level.

Double-labeling immunofluorescence assay

Double-labeling immunofluorescence staining was performed on the tissue microarrays mentioned above using a TSA fluorescence kit. Briefly, the microarrays were incubated with the primary antibodies against CD68 (Cat. ab213363, Abcam) and PPT1 (Cat. ab89022, Abcam), followed by visualization with Alexa Fluor 488 and CY3. Later, the microarrays were scanned and analyzed using CaseViewer software. $PPT1^{+}CD68^{+}$ cell infiltration level was evaluated as the number of positive cell numbers. The median value was served as a cut-off value to divide patients with HCC into high and low $PPT1^{+}CD68^{+}$ macrophage infiltration groups. Patient with HCC were divided into $PPT1^{+}CD68^{+}$ cells enriched group or $PPT1^{-}CD68^{+}$ cells enriched group based on the infiltration percentage of these cells.

CyTOF

Fresh tumor tissues excised from eight patients with HCC were prepared into single cell suspensions and then incubated with 42 metal-conjugated antibodies. Subsequently, signal detection was performed in the Helios3 CyTOF system by PLTTech (Hangzhou, China). The CyTOF data was then normalized and analyzed on the Cytobank platform. Unsupervised clustering and t-SNE dimensionality reduction were performed based on the expression profiles of these markers using the 'cytofkit' package in R software to identify cell types. Detailed antibody information was summarized in online supplemental table 1.

Cell lines

The murine HCC cell lines Hepa1-6 and the human monocytic-leukemia cell line THP-1 were obtained from the Stem Cell Bank, Chinese Academy of Science (Shanghai, China). HCC cells and THP-1 cells were maintained in the Dulbecco's modified Eagle's medium (DMEM) and Roswell Park Memorial Institute (RPMI) 1640 medium with 10% fetal bovine serum (FBS) and 100 mg/mL penicillin and streptomycin, respectively.

RNA isolation and transcriptome sequencing

RNA was extracted from the indicated cells using the TRIzol reagent (Invitrogen, USA) and sent to Agilent 2100 bioanalyzer for integrity check. After enrichment and random cleavage, fragmented messenger RNA (mRNA) was reversely transcribed into complementary DNA (cDNA) and further amplified by PCR to construct cDNA library. Later, transcriptome sequencing was performed on an HiSeq X platform (Illumina).

Quantitative real-time PCR

After extracted from cells as described above, RNA was reverse-transcribed into cDNA using the PrimeScript RT reagent kit (Takara, Japan) according to the standard procedure. A PCR reaction system was established using cDNA, primers, and SYBR Green Master Mix according to the manufacturer's instructions and run on an ABI Prism 7500 Sequence Detection System (Applied Biosystems). The relative mRNA level of the target gene was calculated using the ΔΔCt method with housekeeping gene *GAPDH* as control. The sequences of the primers were listed in online supplemental table 2.

Western blot assay

Proteins were extracted from cultured cells using radioimmunoprecipitation assay (RIPA) buffer and quantified using the Bicin-choninic Acid (BCA) assay kit. After thermal denaturation, proteins were separated by sodium dodecyl sulfate polyacrylamide gel electrophoresis (SDS-PAGE) and transferred onto the PolyVinylideneFluoride (PVDF) membranes according to the standard procedure. Later, bands were blocked with 5% skim milk and incubated overnight with the corresponding primary antibody. Finally, the blots were exposed with chemiluminescence reagents after incubating with the HRP-conjugated secondary antibody. The primary antibodies were summarized in online supplemental table 3.

Flow cytometry

Cultured cells were trypsinized using trypsin and tumors harvested from mouse models were shredded and digested using collagenase to obtain single cell suspension. Later, after stained with fixable viability dye and permeabilized, cells were incubated with fluorochrome-conjugated

antibodies in the dark for 30 min and further sent to the BD FACSAria III Flow Cytometer for flow cytometry. The results were analyzed using the FlowJo software. The antibodies used were shown in online supplemental table 3.

Animal studies

In vivo tumorigenesis assay was performed with male C57BL/6J mice aged 6 weeks. Briefly, mouse HCC cells Hepa1-6 (1×10^6) were subcutaneously injected into the right flank of each mouse. Once palpable, the following treatment commenced and mice were randomly divided into four groups (five mice per group): for PPT1 inhibition, mice were injected intraperitoneally with DC661 3 mg/kg (Cat. HY-111621, MedChemExpress) or vehicle control daily; for anti-PD-1 therapy, mice were treated intraperitoneally with two times per week doses of 100 µg anti-mouse PD-1 antibody (Cat. BP0273; Bio X Cell) or IgG isotype control. Tumor size was measured using vernier caliper and calculated as $0.5\times\text{length}\times\text{width}^2$. All experiments were performed in accordance with the guidelines for care and use of laboratory animals and approved by the Zhongshan Hospital Institutional Animal Care and Ethics Committee (ID: 2021–30).

Statistical analysis

Numerical variables were shown as mean±SD and differences between groups was tested using Student's t-test, one-way analysis of variance or Mann-Whitney U test as appropriate. Categorical variables were presented as n (%) and constituent ratio between groups was compared using Pearson χ^2 and Fisher's exact test. Survival curves were plotted by Kaplan-Meier method and compared with a log-rank test. All analyses were performed with SPSS V.22.0 (IBM, Armonk, New York, USA) and R software (V.4.0.0) with a two-tailed p value less than 0.05 considered statistically significant.

RESULTS

Single-cell RNA sequencing analyses identify seven valuable macrophage-specific marker genes associated with prognosis in HCC

To determine specific transcriptomic landscapes of macrophages in the microenvironment of HCC, we first employed a public data set (GSE125449) containing single-cell RNA sequencing data of 12 patients with liver cancer (Set 1) for bioinformatics analyses. After t-SNE analysis of the top 20 linearly uncorrelated principal components, we successfully obtained 15 cell subclusters in a two-dimensional space and annotated them into seven cell types based on the canonical marker genes, including malignant cell, endothelial cell, $CD8^+$ T cell, B cell, fibroblast, monocyte, and macrophage (figure 1A). Besides, clustering analysis revealed significantly different transcriptional profiles among these single cell subclusters (figure 1B). We then extracted 427 characteristic maker genes of cluster 7 (macrophages) for further analysis. Gene Ontology (GO) demonstrated that these genes were mainly involved in immunomodulatory processes and possessed molecular functions such as major histocompatibility complex (MHC) binding, immunoglobulin binding, and pattern recognition receptor activity (figure 1C). We next confirmed that these genes were macrophage-specific, as evidenced by Kyoto Encyclopedia of Genes and Genomes (KEGG) analysis showing that they were primarily responsible for phagocytosis, and antigen processing and presentation (figure 1D). To investigate which macrophage-specific genes have an essential impact on the disease progression and the clinical outcome of HCC, we performed univariate Cox proportional hazards regression analysis of these genes in the TCGA-LIHC cohort containing 374 patients with liver cancer, and then subjected candidate prognosis-associated genes with statistical significance ($p<0.05$) to the least absolute shrinkage and selection operator (LASSO) analysis. These analyses finally identified seven of the most valuable genes (*PPT1*, *H2AFY*, *PGD*, *YBX1*, *HSPH1*, *TUBA4A*, and *HSPD1*) with 1000-fold cross-validation (figure 1E–G). Taken together, our single-cell RNA sequencing analyses reveal a panel of genes that may play a role in macrophages and affect the progression of HCC.

PPT1 is upregulated in HCC tissues and mainly expressed in macrophages

We next investigated the expression distribution of these genes in the above single cell subclusters. Bubble and t-SNE plots showed that only PPT1 was highly expressed in macrophages (Cluster 7), moderately expressed in monocytes (Cluster 8) and endothelial cells (Cluster 14), while hardly expressed in other cells (figure 2A,B). This finding was further supported by the GSE125449 Set 2 cohort containing seven patients (online supplemental figure A–C). In addition, macrophage subset analysis indicated that M2-like macrophages tended to highly express PPT1 (online supplemental figure 2). Hence, we focused on this molecule for further analyses. Expression analyses in the TCGA-LIHC cohort demonstrated that PPT1 levels were upregulated in tumor tissues compared with peritumor tissues, and increased as disease progression (figure 2C,D). In addition, PPT1 expression was positively correlated with the macrophage infiltration calculated by the CIBERSORT algorithm (R=0.11; figure 2E). The elevated PPT1 expression in tumor tissues and the positive association between PPT1 level and macrophage infiltration were also validated in our own patient with HCC cohort, as indicated by the IHC staining of PPT1 and CD68 (figure 2F,G and online supplemental table S4). In addition, double-labeling immunofluorescence assay revealed that PPT1 mainly co-localized with CD68 in HCC tissues, with a median percentage of 70.0% of PPT1 expressing cells co-localizing in 169 HCC sections (figure 2H and online supplemental figure 3A). Collectively, these results suggest that PPT1 is upregulated in HCC and mainly expressed in macrophages.

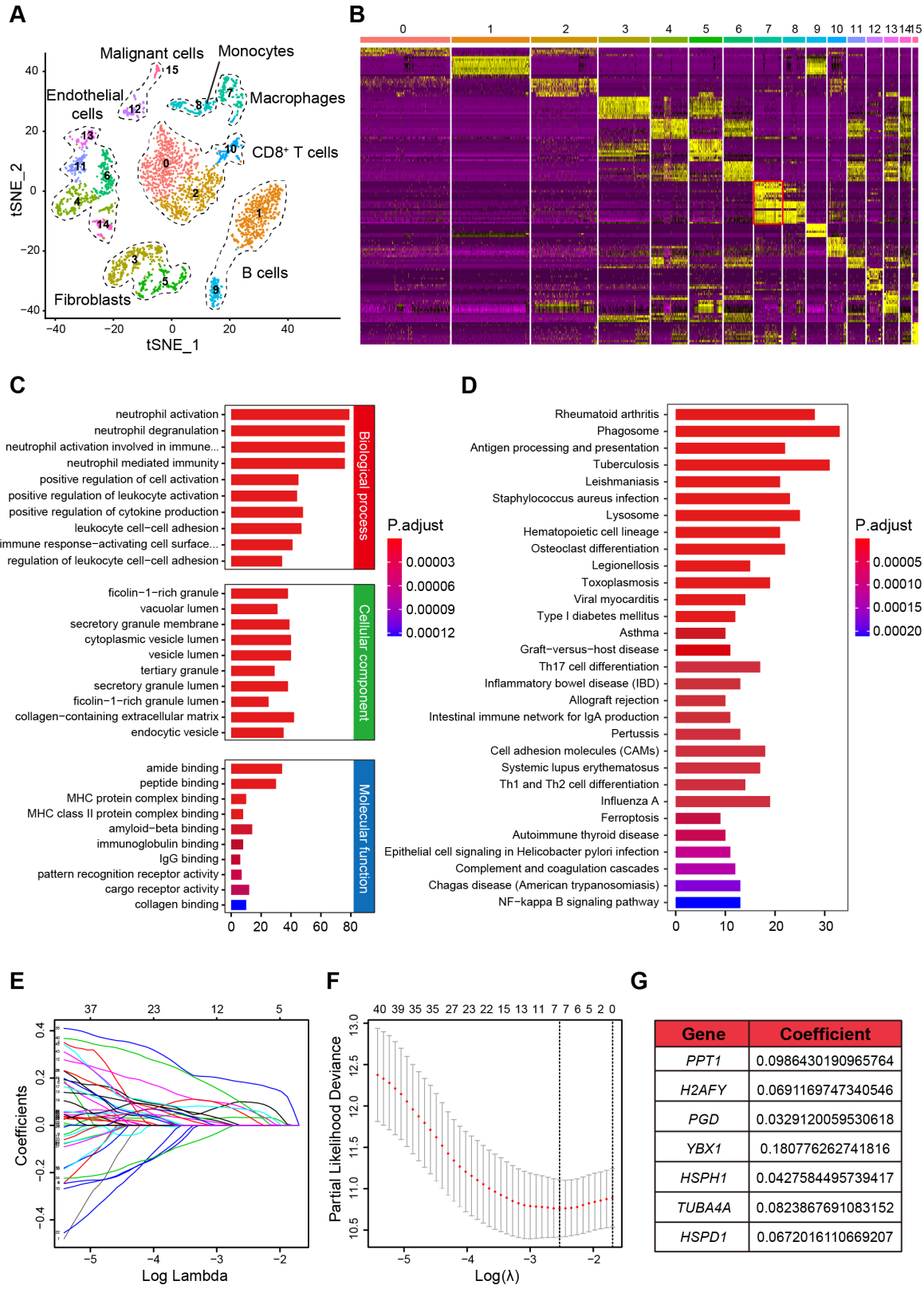

Gene	Coefficient
PPT1	0.0986430190965764
H2AFY	0.0691169747340546
PGD	0.0329120059530618
YBX1	0.180776262741816
HSPH1	0.0427584495739417
TUBA4A	0.0823867691083152
HSPD1	0.0672016110669207

Figure 1 Single-cell RNA sequencing analyses identify seven valuable macrophage-specific marker genes associated with prognosis in HCC. (A) t-SNE plot of 3299 single cells from 12 patients with liver cancer in GSE125449 cohort. (B) Heatmap of marker genes in each single cell subcluster based on the clustering analysis. (C and D) GO and KEGG analyses of 427 maker genes of macrophages (Cluster 7). (E–G) Identification of the most valuable macrophage-specific genes associated with prognosis in HCC using the LASSO analysis with 1000-fold cross-validation in TCGA-LIHC cohort. GO, gene ontology; HCC, hepatocellular carcinoma; KEGG, Kyoto Encyclopedia of Genes and Genomes; LASSO, least absolute shrinkage and selection operator; MHC, major histocompatibility complex; NF, nuclear factor; TCGA-LIHC, the cancer genome atlas liver hepatocellular carcinoma; t-SNE, t-distributed stochastic neighbor embedding.

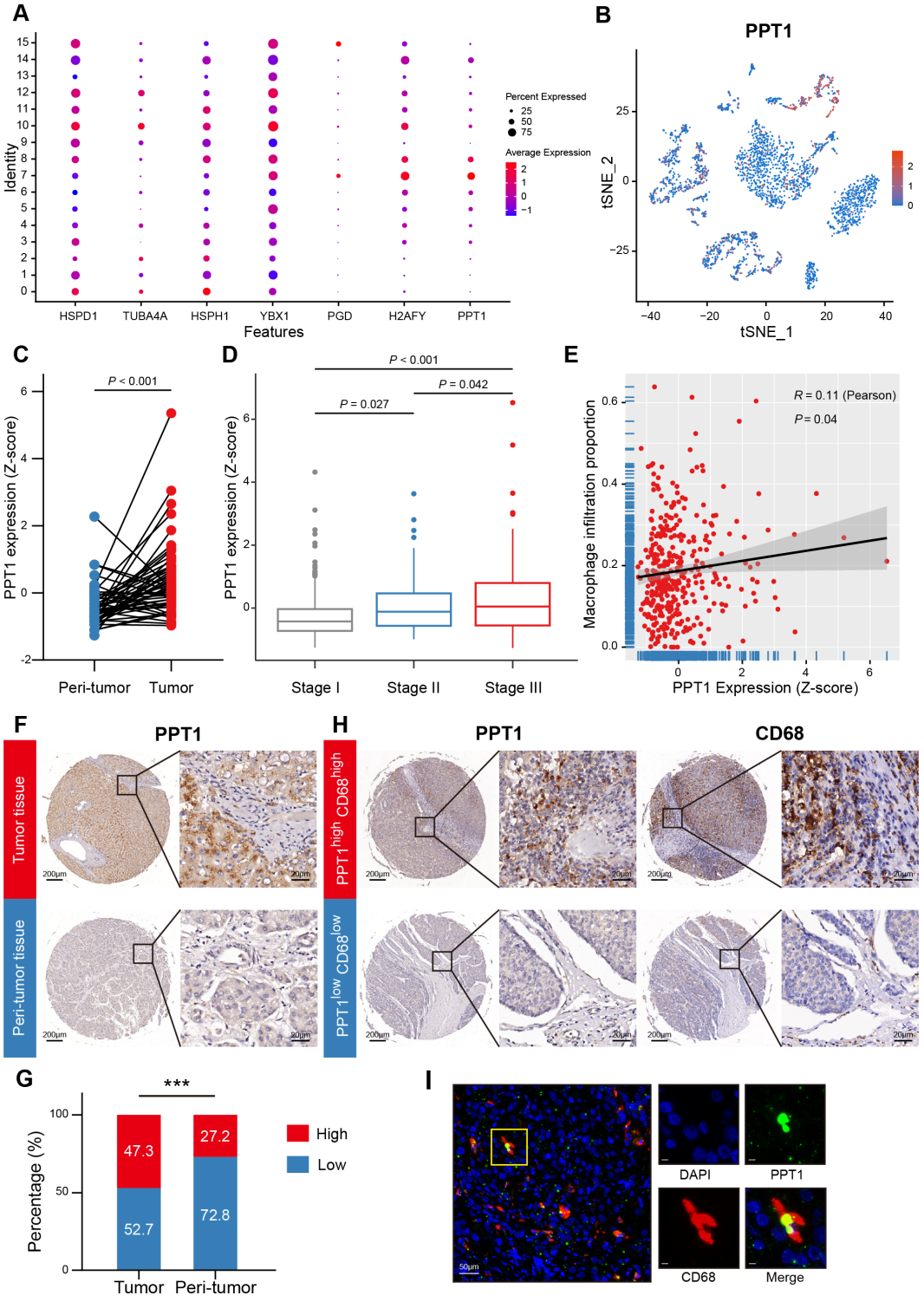

Figure 2 PPT1 is upregulated in HCC tissues and mainly expressed in macrophages. (A) Bubble plot of the expression levels of the seven genes in each single cell subcluster. (B) t-SNE plot of all 3299 single cells colored by the expression level of PPT1. (C) Standardized transcript level of PPT1 in HCC tissues versus matched peritumor tissues (n=50) in TCGA-LIHC cohort. Paired Student's t-test. (D) Standardized transcript level of PPT1 in tumor tissues in different TNM stages of patients with HCC (n=374). One-way ANOVA test. (E) Pearson correlation analysis of neoplastic PPT1 transcript level with the infiltration proportion of macrophage. (F) Representative IHC images of PPT1 in HCC tissues and peritumor tissues. Scale bar, 200 µm (left) and 20 µm (right). (G) IHC expression pattern of PPT1 in HCC tissues versus peritumor tissues (n=169). Paired Student's t-test. (H) Representative IHC images of PPT1 and CD68 for different infiltration levels of $PPT1^{+}$ macrophages in HCC tissues. (I) Representative images of immunofluorescence co-staining of CD68 (red) and PPT1 (green) in HCC tissues. Scale bar, 50 µm (left) and 20 µm (right). ANOVA, analysis of variance; HCC, hepatocellular carcinoma; IHC, immunohistochemistry; PPT1, palmitoyl-protein thioesterase 1; TCGA-LIHC, the cancer genome atlas liver hepatocellular carcinoma; TNM, tumor-node-metastasis; t-SNE, t-distributed stochastic neighbor embedding.

Infiltration of PPT1$^+$ macrophages is closely associated with prognosis in patients with HCC

We then examined the prognostic value of PPT1$^+$ macrophages in patients with HCC using the Kaplan-Meier method. Survival analyses revealed that high PPT1 expression was associated with short OS durations in our patient cohort (figure 3A). Besides, patients with high CD68 level experienced worse OS than those with low CD68 level (online supplemental figure 3B). Of note, we found that tumor with low expression of both PPT1 and CD68 represented the best OS rate in patients with HCC (figure 3B). We further grouped patients with HCC according to the PPT1$^+$CD68$^+$ macrophage infiltration level based on the immunofluorescence staining results. As illustrated in figure 3C, the OS duration of patients with HCC with high PPT1$^+$CD68$^+$ macrophage infiltration was shorter than that of patients in the low infiltration group. Moreover, patients with HCC enriched with PPT1$^+$CD68$^+$ macrophages experienced a shorter OS duration than those enriched with PPT1$^-$CD68$^+$ macrophages (online supplemental figure 3C). The association of high PPT1 expression, high macrophage infiltration with poor OS and disease-free survival (DFS) of HCC was also observed in the TCGA-LIHC cohort (figure 3D,E). Consistently, patients with HCC with low intratumoral PPT1$^+$ macrophages infiltration tended to have the best DFS and OS durations (figure 3F). In addition, Cox proportional hazard regression models demonstrated that high intratumoral expression of both PPT1 and CD68 was an independent risk factor for OS in patients with HCC from our cohort (figure 3G). Hence, infiltration of PPT1$^+$ macrophages in tumor has a negative influence on the clinical outcomes of patients with HCC.

Intratumoral PPT1$^+$ macrophages correlate with immune exhaustion contexture and exhibit immunosuppressive phenotype in HCC microenvironment

To understand the mechanisms underlying the dismal prognosis caused by high PPT1$^+$ macrophage infiltration, we then scrutinized the immune infiltrates and functional profiles between HCC tumors with high and low infiltration of PPT1$^+$ macrophages using the CyTOF assay. Clustering analysis identified 35 cell subsets in eight HCC tumors, with PPT1 expression mainly distributed in macrophages and T-cell subsets (figure 4A,B). Intriguingly, tumor with high level of intratumoral PPT1$^+$ macrophages possessed significantly increased CD8$^+$ T-cell infiltration and slightly elevated CD4$^+$ regulatory T cell (Treg) levels, while the proportions of other immune cell types in CD45$^+$ cells were comparable between the two groups (figure 4C,D). We further analyzed the subpopulation of CD8$^+$ T cells and found that the C04 was the predominant CD8$^+$ T-cell subset positively associated with the PPT1$^+$ macrophage infiltration (figure 4E,F). In addition, cellular function analysis showed that the expression of PD-1 was increased in C04 subset from the high PPT1$^+$ macrophage infiltration group, suggesting that PPT1$^+$ macrophages may promote the function exhaustion of this CD8$^+$ T-cell subpopulation (figure 4G). We also explored the association between intratumoral PPT1 expression and the immune landscapes of HCC microenvironment in TCGA-LIHC cohort. Clustering analysis of ssGSEA revealed that tumors with high PPT1 level tended to have more immunological activity than those with low PPT1 expression (online supplemental figure 4A). Consistently, neoplastic PPT1 level seemed to be positively correlated with the infiltration of CD8$^+$ T cells, which was also validated using the CIBERSORT algorithm (online supplemental figure 4B–G). Besides, we also found enhanced checkpoint activity, T cell co-inhibition, and antigen presenting cell (APC) co-inhibition and attenuated type II interferon (IFN)-γ response in PPT1 high expression group (online supplemental figure 4H).

We next examined the function status of PPT1$^+$ macrophages in HCC tumor. Out of the six macrophage subsets, five clusters (C27–C31) were associated with PPT1 expression (figure 4E). PPT1$^+$ macrophages within HCC tissues exposed higher levels of galectin-9 (the ligand for T-cell checkpoint TIM-3), CD172a (the ligand for macrophage phagocytic checkpoint CD47), and CCR2 (a marker of M2 type macrophage) compared with the PPT1$^-$ macrophages (figure 4H,I). In addition, CD80 and CCR7, two markers of M1 type macrophage, showed decreased expression in PPT1$^+$ macrophages. Taken together, these results demonstrated that PPT1$^+$ macrophages exhibit an immunosuppressive status with diminished phagocytosis function, and may affect the tumor infiltration and functional status of a subset of CD8$^+$ T cells, contributing to an immune exhaustion contexture in HCC microenvironment.

Inhibition of PPT1 by DC661 reverses the immunosuppressive phenotype of macrophages

Having established a connection between PPT1 expression and the immunosuppressive phenotype of macrophages in HCC, we next investigated the mechanism by which inhibition of PPT1 was affecting macrophages. By performing RNA sequencing, we identified 335 significantly upregulated genes and 452 downregulated genes in THP-1-differentiated macrophages treated with the PPT1 inhibitor DC661 compared with the control group (figure 5A). GO analysis indicated that these differential genes were mainly involved in cell migration, chemotaxis, receptor signaling pathway and cytokine activity (figure 5B). In addition, KEGG analysis demonstrated that DC661 treatment could activate several inflammation-related signaling pathways including the TNF, IL-17, NF-κB, and Toll-like receptor signaling pathways, while inhibit MAPK, Ras, PI3K-Akt signaling pathways and EGFR tyrosine kinase inhibitor resistance (figure 5C). We also found that the transcription of some genes involved in M2 polarization, Treg recruitment, and T-cell exhaustion, such as IL-24, MAF, CD209, CCL28, PDCD1, and IL-10, was inhibited by DC661, while the expression of genes involved in tumor killing, T-cell chemotaxis, and neutrophil recruitment, such as TNF, CCL4, CCL5,

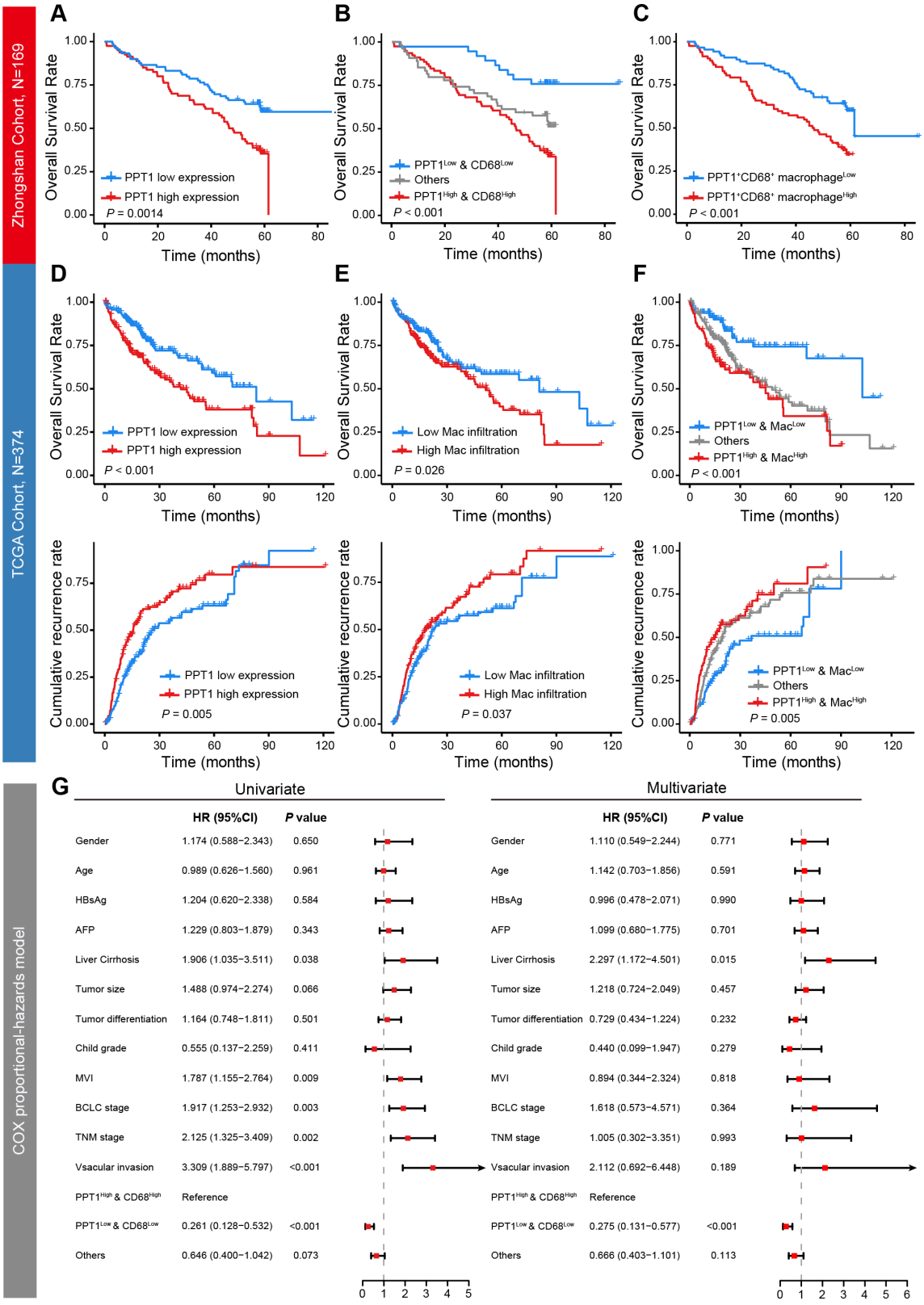

Figure 3 The prognostic value of PPT1$^+$ macrophages infiltration in HCC. (A–B) OS curves for patients with HCC with high and low expression of PPT1 or PPT1/CD68 co-expressions based on IHC staining in our patient cohort (n=169). (C) OS curve for patients with HCC with high and low PPT1$^+$CD68$^+$ macrophage infiltration based on double-labeling immunofluorescence staining in our patient cohort (n=169). (D–F) OS and DFS curves for patients with HCC with high and low mRNA level of PPT1, infiltration level of macrophages or PPT1$^+$ macrophages in TCGA-LIHC cohort (n=374). Log-rank test. (G) Forest plots for univariate and multivariate Cox proportional hazards regression models of OS in patients with HCC from our patient cohort. DFS, disease-free survival; HCC, hepatocellular carcinoma; IHC, immunohistochemistry; mRNA, messenger RNA; OS, overall survival; PPT1, palmitoyl-protein thioesterase 1; TCGA-LIHC, the cancer genome atlas liver hepatocellular carcinoma.

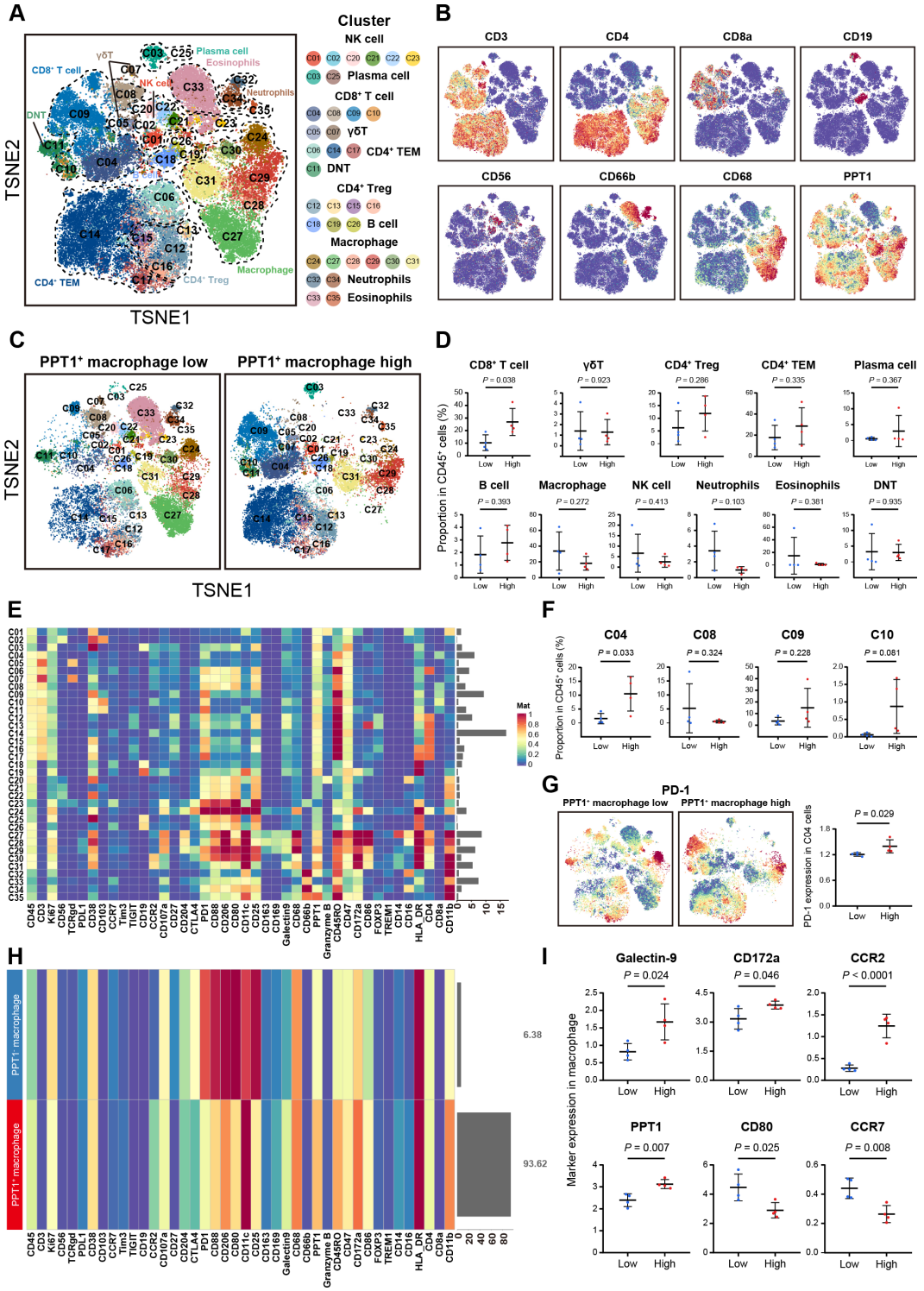

Figure 4 PPT1⁺ macrophages correlate with immune exhaustion contexture and exhibit immunosuppressive phenotype in HCC microenvironment. (A) t-SNE plot of CD45⁺ cells in the tumor from eight patients with HCC based on CyTOF results. Cell cluster type was annotated according to the known marker expression. (B) t-SNE plot of CD45⁺ cells colored by the levels of CD3, CD4, CD8a, CD19, CD56, CD66b, CD68, and PPT1. (C) t-SNE plot of CD45⁺ cells in the tumors from PPT1⁺ macrophage low and high infiltration groups. (D) Proportion of the indicated immune cell types in CD45⁺ cells in the two groups. (E) Heatmap of 42 markers expressed in each cell cluster. (F) Proportion of the indicated CD8⁺ T cell subsets in CD45⁺ cells in the two groups. (G) Left: t-SNE plot of CD45⁺ cells colored by the level of PD-1. Right: PD-1 expression of C04 subset in the indicated groups. (H) Heatmap of 42 markers expressed in PPT1-positive and negative macrophages. (I) The expression level of galectin-9, CD172a, CCR2, PPT1, CD80, and CCR7 in PPT1-positive and negative macrophages. Mann-Whitney U test. CyTOF, cytometry by time-of-flight; DNT, double-negative T cell; HCC, hepatocellular carcinoma; NK, natural killer; PD-1, programmed death receptor 1; PPT1, palmitoyl-protein thioesterase 1; TEM, effector memory T cell; Treg, regulatory T cell; t-SNE, t-distributed stochastic neighbor embedding.

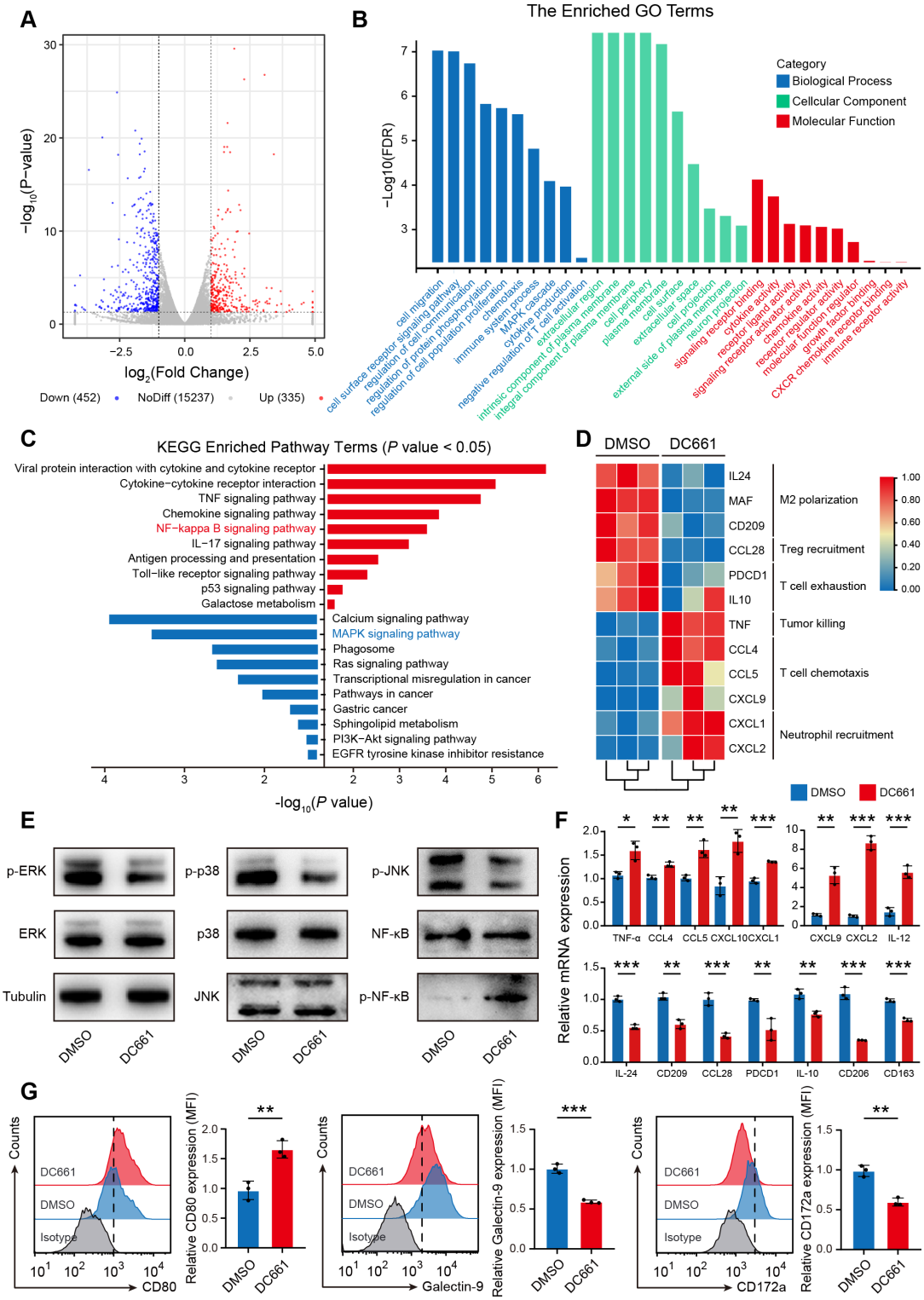

Figure 5 Inhibition of PPT1 by DC661 reverses the immunosuppressive phenotype of macrophages. (A) Volcano plot of differentially expressed genes between DMSO and DC661 treatment groups. (B) Gene Ontology analysis of differentially expressed genes between DMSO and DC661 treatment groups. (C) KEGG analysis of differentially expressed genes between DMSO and DC661 treatment groups. (D) Heatmap of the indicated genes in DMSO and DC661 treatment groups. (E) Western blot of MAPK and NF-κB signaling pathways in THP-1-differentiated macrophages treated with the DMSO and DC661. (F) qPCR analyses of the indicated genes in DMSO and DC661 treatment groups. (G) Flow cytometry analysis of CD80, galectin-9, and CD172a expression in the indicated groups. *p<0.05, **p<0.01, and ***p<0.001, Student's t-test. DMSO, dimethyl sulfoxide; EGFR, epidermal growth factor receptor; ERK, extracellular signal-regulated kinase; FDR, false discovery rate; GO, gene ontology; IL, interleukin; JNK, c-Jun N-terminal kinase; KEGG, Kyoto Encyclopedia of Genes and Genomes; MAPK, mitogen-activated protein kinase; MFI, median fluorescence intensity; NF, nuclear factor; NF-κB, nuclear factor kappa B; PPT1, palmitoyl-protein thioesterase 1; qPCR, quantitative real-time PCR; TNF, tumor necrosis factor.

CXCL9, CXCL1, and CXCL2, was enhanced by DC661 (figure 5D). Activation of NF-κB pathway and inhibition of MAPK pathway induced by DC661 in macrophages were further confirmed by WB, and transcriptional regulation of immune-related genes in macrophages by DC661 was also validated by quantitative PCR (figure 5E,F). In addition, DC661 treatment could increase CD80 membrane expression and decrease galectin-9 and CD172a levels in macrophages (figure 5G). These results suggested that inhibition of PPT activity with DC661 attenuates the immunosuppressive phenotype of macrophages.

DC661 enhances the efficacy of anti-PD-1 antibody in HCC in vivo

The above results drove us to investigate whether PPT1 inhibition could potentiate the therapeutic efficacy of immunotherapy in HCC. We constructed Hepa1-6-derived subcutaneous HCC mouse models and treated them with IgG, anti-PD-1 antibody, DC661, and anti-PD-1 antibody combined with DC661, respectively (figure 6A). During treatment, DC661, anti-PD-1 antibody and combination therapy all significantly restricted the growth of subcutaneous tumors (figure 6B). Besides, tumors harvested at the endpoint of experiment were much smaller for combination therapy than monotherapies, along with a significant decrease in the expressions of PPT1 and PD-1 (figure 6C,D and online supplemental figure 5A). To further understand the mechanism underlying the enhanced antitumor efficacy of combined therapy, we dissected the tumor immune infiltration landscape of Hepa1-6 subcutaneous tumors. As shown by flow cytometric analyses, mice administered with combination therapy had significantly increased tumor infiltrations of MHC-II$^+$ M1 macrophages and CD8$^+$ T cells compared with the monotherapies and the control (figure 6E,F). Finally, no notable hepatic or renal toxicity was observed at the endpoint of the study for both monotherapies and combination therapy (figure 6G). Collectively, these findings highlighted that PPT1 inhibition by DC661 may potentiate the therapeutic efficacy of anti-PD-1 therapy in HCC.

DISCUSSION

Macrophages, one of the major immune cell types in the HCC microenvironment, act as a double-edged sword in hepatocarcinogenesis. Hepatic macrophages can attenuate the loss of CD4$^+$ T cells caused by dysregulation of lipid metabolism to delay HCC.[20] Besides, cannabinoid receptor 2 expressed in macrophages can promote the recruitment of T cells to induce antitumor response.[21] On the other hand, macrophages in HCC often undergo a re-education process into immunosuppressive TAMs, which accelerate the development of HCC.[22–24] The heterogeneous phenotypes of macrophages and its inextricable connection with tumor microenvironment (TME) highlight the importance of a better understanding of the crucial macrophage subpopulations and their impacts on immune contexture. Here, using multiple high-throughput single-cell analyses, we identified a previously undescribed PPT1$^+$ macrophage subset and elucidated its immune association and clinical significance in HCC.

The relationship between the PPT1 expression level in tumor and the prognosis of HCC has been recognized, and some PPT1 inhibitors such as DC661 and GNS561 have been found to inhibit HCC or enhance the sensitivity of sorafenib.[11 14] In line with this, we observed an elevated expression of PPT1 in HCC tissues and a negative effect of PPT1 on the clinical outcomes of patients with HCC. More importantly, our findings shed insight into a predominant expression pattern of PPT1 in the HCC microenvironment. The high expression of PPT1 in macrophages and the best survival duration observed in HCC with low PPT1$^+$ macrophages infiltration suggests that PPT1$^+$ macrophage is an essential macrophage subset that influences the progression of HCC. Several studies have revealed that PPT1 is the pharmacological target of chloroquine derivatives.[13 16] Therefore, our study gives a rationale for antimalarial drugs as a macrophages-targeting therapy in HCC. In addition, our work sets the stage for future studies that may be extrapolated to other types of tumors to investigate whether the high expression of PPT1 in macrophages is ubiquitous in cancers. Finally, we need to point out that since some subpopulations of other immune cells such as T cells also express PPT1, pharmacological inhibition of PPT1 in vivo may exert antitumor effects by targeting other PPT1-expressing cells, and the function of PPT1 in these cells needs to be further investigated.

Another important finding of this study is that the HCC microenvironment with high PPT1$^+$ macrophage infiltration is characterized by high tumor infiltration of a CD8$^+$ T cell subset with increased PD-1 expression. The characteristics of the tumor immune infiltrates have been recognized as an important factor that influences response to immunotherapy.[8] Currently, TME can be classified into three categories according to the composition and function status of immune infiltrates obtained from moderate-resolution data, namely infiltrated-excluded, infiltrated-inflamed, and infiltrated-tertiary lymphoid structure.[8] We presume that the PPT1$^+$ macrophage-enriched HCC microenvironment resembles the infiltrated-inflamed TME, which is characterized by high infiltrations of exhausted cytotoxic lymphocytes and immunosuppressive leukocytes. This type of TME is considered to have a high response to ICB.[8] The enhanced antitumor effect of anti-PD-1 antibody against HCC induced by DC661 in our in vivo experiments fully supports this hypothesis. Thus, our study reveals an important role of PPT1 in mediating the interaction of macrophages with surrounding cells to shape the immunosuppressive TME, and suggests that PPT1 level and PPT1$^+$ macrophages may be potent predictive biomarkers of immunotherapy response for HCC. Besides, a study in melanoma reported that PPT1 inhibitors can promote the secretion of IFN-β in macrophages to enhance T cell-mediated cytotoxicity

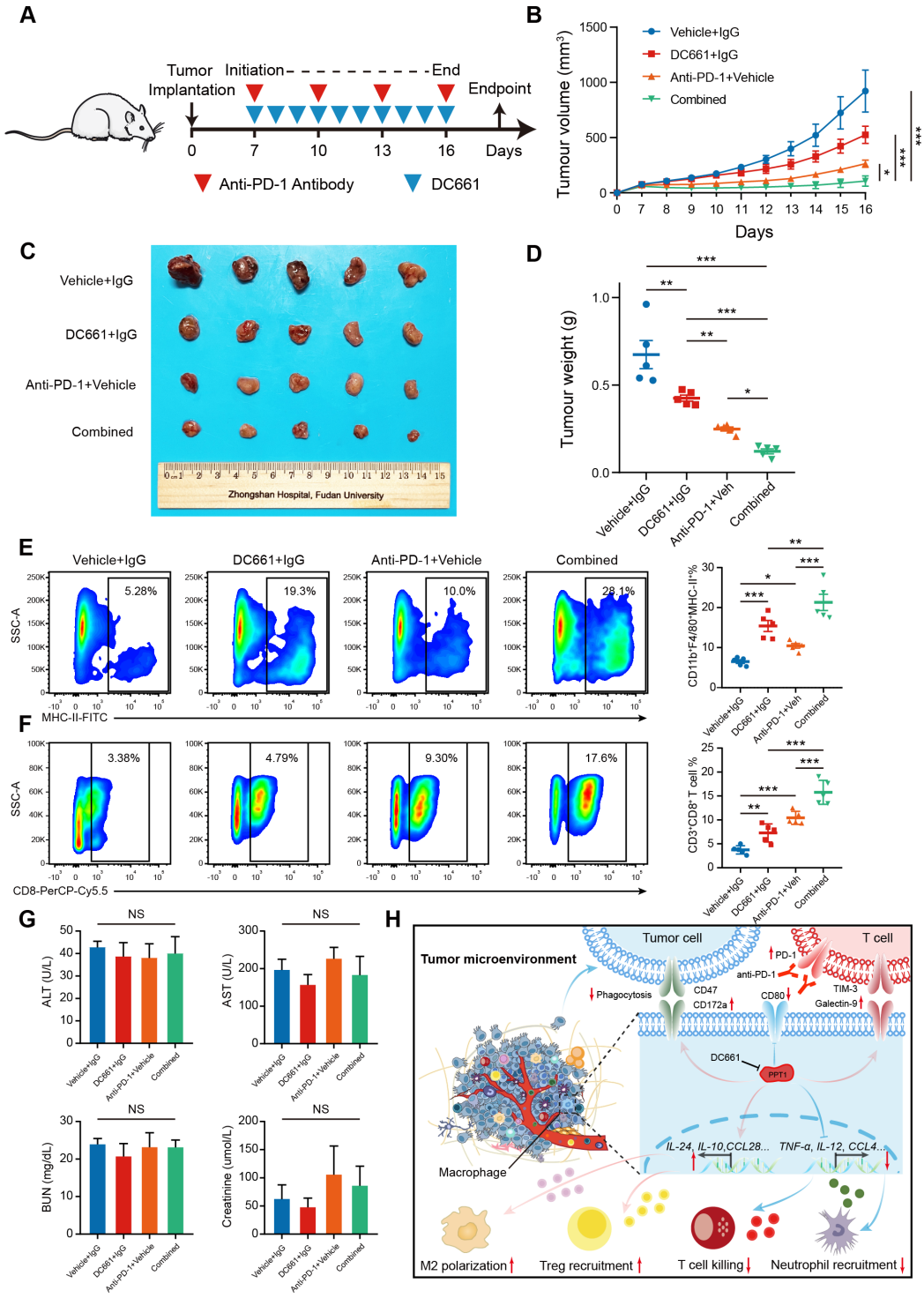

Figure 6 DC661 enhances the efficacy of anti-PD-1 antibody in HCC in vivo. (A) Schematic showing the schedule of anti-PD-1 and PPT1 inhibitor DC661 treatment in mice bearing Hepa1-6 tumors. (B) Volumes of subcutaneous tumors in each group during treatment. (C) Gross appearance of the subcutaneous HCC tumors from the indicated treatment groups. (D) The tumor weight of each group at the endpoint. (E–F) Flow cytometry analyses of the tumor infiltration percentage of $CD11b^+F4/80^+MHC\text{-}II^+$ macrophages and $CD3^+CD8^+$ T cells in each group. (G) Effects of anti-PD-1 and DC661 on liver and kidney functions of mice with subcutaneous HCC tumors at study endpoint. (H) Schematic diagram depicting the regulatory role of PPT1 in macrophage and the microenvironment immune landscapes of HCC. PPT1 can upregulate the membrane level of CD172a and galectin-9 but downregulate CD80 in macrophages, thereby impairing its phagocytosis and inhibiting the killing ability of T cells. Besides, by regulating the transcription of immune-related cytokines, PPT1 promotes M2 polarization, Treg recruitment, and inhibits the recruitment of neutrophils. *p<0.05, **p<0.01, and ***p<0.001, one-way ANOVA with a post hoc LSD test. ALT, alanine transaminase; ANOVA, analysis of variance; AST, aspartate aminotransferase; BUN, blood urea nitrogen; FITC, fluorescein isothiocyanate; HCC, hepatocellular carcinoma; LSD, least significant difference; MHC, major histocompatibility complex; PD-1, programmed death receptor 1; PPT1, palmitoyl-protein thioesterase 1; SSC, side scatter; Treg, regulatory T cell.

and the efficacy of ICB.[15] Hence, based on our results, adjuvant PPT1 inhibitor may disrupt the immunosuppressive TME shaped by macrophages and potentiate the therapeutic effect of immunotherapy in HCC, which warrants further investigations.

In addition, we observed that PPT1$^+$ macrophages had decreased CD80 and increased CD172a and galectin-9 expression, suggesting that PPT1 impaired the phagocytosis function and enhanced immunosuppressive function of macrophages. Consistently, a study demonstrated that genetic and pharmacological PPT1 inhibitions lead to the M2 to M1 phenotype switch in macrophages, suggesting a determinant role of PPT1 in the immune function of macrophages.[15] Besides, we observed that many immune-related cytokine or chemokine profiles in macrophages, as well as MAPK and NF-κB pathways, were greatly affected by DC661 treatment. Transcriptional alterations of these cytokines may be key mediators of functional remodeling in macrophages as well as their impact on surrounding cells.[25–27] These pathways, also, may be important modulators of gene transcription as described above. Some studies have reported that PPT1 is involved in the mammalian target of rapamycin (mTOR) pathway activation and lysosomal catabolism by its depalmitoylase activity.[14 16] Palmitoylation modifications play an important regulatory role in protein localization and function, as well as in tumorigenesis.[28–30] Therefore, protein palmitoylation modifications regulated by PPT1 may be a potential mechanism underlying the effect of PPT1 on signaling pathways and immune phenotypes in macrophages.

However, considering that the present study did not elucidate the specific mechanisms underlying the role of PPT1$^+$ macrophages in the TME immune landscape, basic studies based on in vivo and in vitro experiments are needed in the future. Besides, a large-scale and multicentral patient cohort is highly desirable to validate our findings. The therapeutic effect of PPT1 inhibitors combined with ICB in HCC also requires further investigation.

CONCLUSION

In conclusion, our study provides the first insight into the enriched expression of PPT1 in macrophages in HCC and identifies the infiltration level of PPT1$^+$ macrophage as an independent risk factor for OS in HCC. PPT1$^+$ macrophages exhibit a highly immunosuppressive phenotype and shift the HCC microenvironment into a tumor-promoting context (figure 6H). Targeting PPT1 may potentiate the therapeutic efficacy of immunotherapy in HCC.

Author affiliations
[1]Department of Liver Surgery and Transplantation, Liver Cancer Institute, Zhongshan Hospital, Fudan University, Key Laboratory of Carcinogenesis and Cancer Invasion, Ministry of Education, Shanghai, China
[2]Key Laboratory of Whole-Period Monitoring and Precise Intervention of Digestive Cancer of Shanghai Municipal Health Commission, Shanghai, China
[3]Biomedical Research Centre, Zhongshan Hospital Fudan University, Shanghai, China
[4]Institute of Fudan-Minhang Academic Health System, Minhang Hospital, Fudan University, Shanghai, China

Contributors JW, SL and QZ designed and analyzed data, performed experiments, and wrote the manuscript. WX, MX and DG contributed to the acquisition and interpretation of data. YShen and YY provided patient tissue samples and clinical data. YShi and QD provided scientific input and revised the manuscript. CZ and NR supervised and conceived the entire project. CZ and NR are responsible for the overall content as the guarantors.

Funding This study was supported by grants from the National Natural Science Foundation of China (82073208, 82103521), the Sino-German Mobility Program (M-0603), the Special Foundation for Science and Technology Basic Research Program (2019FY101103), the Shanghai Sailing Program (21YF1407500), China Postdoctoral Science Foundation (2021M690674), and the Shanghai Shen Kang Hospital Development Center New Frontier Technology Joint Project (SHDC12021109).

Competing interests None declared.

Patient consent for publication Not applicable.

Ethics approval The study was reviewed and approved by the Ethics Committee of Zhongshan Hospital, Fudan University (Shanghai, China) (ID: B2021-143R). Participants gave informed consent to participate in the study before taking part.

Provenance and peer review Not commissioned; externally peer reviewed.

Data availability statement All data relevant to the study are included in the article or uploaded as supplementary information. Data are available from The Cancer Genome Atlas (http://cancergenome.nih.gov/) and series GSE125449 in the GEO (Gene Expression Omnibus) website (https://www.ncbi.nlm.nih.gov/geo/). Other data analyzed in this study are included in the article and supplementary materials.

ORCID iDs
Chenhao Zhou http://orcid.org/0000-0002-4800-3249
Ning Ren http://orcid.org/0000-0001-9776-2471

REFERENCES

1 Sung H, Ferlay J, Siegel RL, *et al*. Global cancer Statistics 2020: GLOBOCAN estimates of incidence and mortality worldwide for 36 cancers in 185 countries. *CA Cancer J Clin* 2021;71:209–49.
2 Llovet JM, Kelley RK, Villanueva A, *et al*. Hepatocellular carcinoma. *Nat Rev Dis Primers* 2021;7:6.
3 Kudo M, Finn RS, Qin S, *et al*. Lenvatinib versus sorafenib in first-line treatment of patients with Unresectable hepatocellular carcinoma: a randomised phase 3 non-inferiority trial. *Lancet* 2018;391:1163–73.
4 Nault J-C, Cheng A-L, Sangro B, *et al*. Milestones in the pathogenesis and management of primary liver cancer. *J Hepatol* 2020;72:209–14.
5 El-Khoueiry AB, Sangro B, Yau T, *et al*. Nivolumab in patients with advanced hepatocellular carcinoma (Checkmate 040): an open-label, non-comparative, phase 1/2 dose escalation and expansion trial. *Lancet* 2017;389:2492–502.
6 Mizukoshi E, Kaneko S. Immune cell therapy for hepatocellular carcinoma. *J Hematol Oncol* 2019;12:52.

7 Keenan BP, Fong L, Kelley RK. Immunotherapy in hepatocellular carcinoma: the complex interface between inflammation, fibrosis, and the immune response. *J Immunother Cancer* 2019;7:267.
8 Binnewies M, Roberts EW, Kersten K, *et al*. Understanding the tumor immune Microenvironment (TIME) for effective therapy. *Nat Med* 2018;24:541–50.
9 Gordon S, Plüddemann A, Martinez Estrada F. Macrophage heterogeneity in tissues: Phenotypic diversity and functions. *Immunol Rev* 2014;262:36–55.
10 Tian Z, Hou X, Liu W, *et al*. Macrophages and hepatocellular carcinoma. *Cell Biosci* 2019;9:79.
11 Xu J, Su Z, Cheng X, *et al*. High Ppt1 expression predicts poor clinical outcome and Ppt1 inhibitor Dc661 enhances sorafenib sensitivity in hepatocellular carcinoma. *Cancer Cell Int* 2022;22:115.
12 Luo Q, Li X, Gan G, *et al*. Ppt1 reduction contributes to Erianin-induced growth inhibition in oral squamous carcinoma cells. *Front Cell Dev Biol* 2021;9:764263.
13 Rebecca VW, Nicastri MC, Fennelly C, *et al*. Ppt1 promotes tumor growth and is the molecular target of chloroquine derivatives in cancer. *Cancer Discov* 2019;9:220–9.
14 Brun S, Bestion E, Raymond E, *et al*. Gns561, a clinical-stage Ppt1 inhibitor, is efficient against hepatocellular carcinoma via modulation of lysosomal functions. *Autophagy* 2022;18:678–94.
15 Sharma G, Ojha R, Noguera-Ortega E, *et al*. Ppt1 inhibition enhances the antitumor activity of anti-PD-1 antibody in Melanoma. *JCI Insight* 2020;5:e133225.
16 Rebecca VW, Nicastri MC, McLaughlin N, *et al*. A unified approach to targeting the Lysosome's Degradative and growth signaling roles. *Cancer Discov* 2017;7:1266–83.
17 Zhou C, Chen W, Sun J, *et al*. Low expression of WW domain-containing Oxidoreductase Associates with hepatocellular carcinoma aggressiveness and recurrence after curative resection. *Cancer Med* 2018;7:3031–43.
18 Ma L, Hernandez MO, Zhao Y, *et al*. Tumor cell Biodiversity drives Microenvironmental Reprogramming in liver cancer. *Cancer Cell* 2019;36:418–30.
19 Sun Y, Wu L, Zhong Y, *et al*. Single-cell landscape of the Ecosystem in early-relapse hepatocellular carcinoma. *Cell* 2021;184:404–21.
20 Ma C, Kesarwala AH, Eggert T, *et al*. NAFLD causes selective Cd4(+) T lymphocyte loss and promotes Hepatocarcinogenesis. *Nature* 2016;531:253–7.
21 Suk K-T, Mederacke I, Gwak G-Y, *et al*. Opposite roles of Cannabinoid receptors 1 and 2 in Hepatocarcinogenesis. *Gut* 2016;65:1721–32.
22 Liang S, Ma H-Y, Zhong Z, *et al*. NADPH oxidase 1 in liver Macrophages promotes inflammation and tumor development in mice. *Gastroenterology* 2019;156:1156–72.
23 Delire B, Henriet P, Lemoine P, *et al*. Chronic liver injury promotes Hepatocarcinoma cell seeding and growth, associated with infiltration by Macrophages. *Cancer Sci* 2018;109:2141–52.
24 Ambade A, Satishchandran A, Saha B, *et al*. Hepatocellular carcinoma is accelerated by NASH involving M2 macrophage polarization mediated by Hif-1Ainduced IL-10. *Oncoimmunology* 2016;5:e1221557.
25 Jeannin P, Paolini L, Adam C, *et al*. The roles of Csfs on the functional polarization of tumor-associated Macrophages. *FEBS J* 2018;285:680–99.
26 Mehla K, Singh PK. Metabolic regulation of macrophage polarization in cancer. *Trends Cancer* 2019;5:822–34.
27 Chen D, Zhang X, Li Z, *et al*. Metabolic regulatory Crosstalk between tumor Microenvironment and tumor-associated Macrophages. *Theranostics* 2021;11:1016–30.
28 Kadry YA, Lee J-Y, Witze ES. Regulation of EGFR signalling by Palmitoylation and its role in tumorigenesis. *Open Biol* 2021;11:210033.
29 Busquets-Hernández C, Triola G. Palmitoylation as a key regulator of Ras localization and function. *Front Mol Biosci* 2021;8:659861.
30 Resh MD. Palmitoylation of hedgehog proteins by hedgehog Acyltransferase: roles in signalling and disease. *Open Biol* 2021;11:200414.